NASA Technical Memorandum 83286

Elastic Deformation Effects on Aerodynamic Characteristics for a High-Aspect-Ratio Supercritical-Wing Model

Judith J. Watson

MAY 1982

NASA

ERRATA

NASA Technical Memorandum 83286

ELASTIC DEFORMATION EFFECTS ON AERODYNAMIC CHARACTERISTICS FOR A HIGH-ASPECT-RATIO SUPERCRITICAL-WING MODEL

Judith J. Watson

May 1982

Please make the following changes:

Page 2, SYMBOLS:
Change units for symbols EI and GJ from kPa to $kN-m^2$

Page 3, "Finite-Element Structural Model," 12th line:
Change units for symbols EI and GJ from kPa to $kN-m^2$

Page 7, last line of result 1:
Change "... angle of attack is 2.085" to "... angle of attack is 0.02085."

Date of issue:
June 1982

NASA Technical Memorandum 83286

Elastic Deformation Effects on Aerodynamic Characteristics for a High-Aspect-Ratio Supercritical-Wing Model

Judith J. Watson
Langley Research Center
Hampton, Virginia

National Aeronautics
and Space Administration

Scientific and Technical Information Office

1982

SUMMARY

The results of an investigation of the effects of elastic deformations on the aerodynamic characteristics for a high-aspect-ratio, force/pressure, supercritical-wing model during wind-tunnel tests are presented.

In this study a finite-element model of the wing was developed and, for conditions corresponding to wind-tunnel test points, experimental aerodynamic loads and theoretical aerodynamic loads were applied to the finite-element model. Comparisons were made between results caused by experimental data loads and analytical data loads, for changes in structural deflections and for changes in aerodynamic characteristics, both caused by increments in wing angle of attack and control-surface deflection.

The results from this study showed good correlation between the analytical and experimental data. They also showed that the deformations were quite small and that the experimental pressure data were not significantly affected by model deformation.

INTRODUCTION

A series of wind-tunnel tests were conducted by the National Aeronautics and Space Administration (NASA) in the Langley Transonic Dynamics Tunnel to investigate the effects of oscillating control surfaces on unsteady aerodynamics. This series of tests was conducted using a model of the high-aspect-ratio (10.76), force/pressure, supercritical-airfoil, semispan wing that has a planform representative of current energy-efficient designs. The results from two of these tests are reported in references 1 and 2. There is concern that the model may experience elastic deformations that may affect the measured wind-tunnel test results, although the wing model was designed to be very rigid. These concerns are addressed in this paper by developing a finite-element structural model and combining it with an aerodynamic model to analytically examine the model deflections caused by steady subsonic and transonic aerodynamic loadings on the wing model. The purpose of the present investigation was to determine the deflection characteristics of the "rigid" wing model and to determine what effect, if any, these deflections had on the aerodynamic characteristics.

SYMBOLS

c_l	section lift coefficient
$c_{m,le}$	section pitching-moment coefficient about the leading edge
C_p	pressure coefficient
C'_p	lifting-surface pressure coefficient, $C_{p,ls} - C_{p,us}$
$\Delta c_l/\Delta\alpha$	increment in section lift coefficient per change in angle of attack, deg^{-1}

$\Delta c_l/\Delta\delta$ increment in section lift coefficient per change in control-surface deflections, deg^{-1}

$\Delta c_{m,le}/\Delta\alpha$ increment in section pitching-moment coefficient about the leading edge per change in angle of attack, deg^{-1}

$\Delta c_{m,le}/\Delta\delta$ increment in section pitching-moment coefficient about the leading edge per change in control-surface deflection, deg^{-1}

$\Delta C'_p/\Delta\alpha$ increment in pressure coefficient per change in angle of attack, deg^{-1}

$\Delta C'_p/\Delta\delta$ increment in pressure coefficient per change in control-surface deflection, deg^{-1}

EI bending stiffness, ~~kPa~~ $KN-m^2$

GJ torsional stiffness, ~~kPa~~ $KN-m^2$

h bending deflection, mm

$\Delta h/\Delta\alpha$ increment in bending deflection per change in angle of attack, mm/deg

$\Delta h/\Delta\delta$ increment in bending deflection per change in control-surface deflection, mm/deg

M Mach number

q free-stream dynamic pressure, kPa

t/c thickness-to-chord ratio

x chordwise or streamwise coordinate, m

x/c fraction of local chord

y spanwise coordinate, m

z vertical coordinate, positive up, m

α angle of attack, deg

δ control-surface deflection, deg

η fraction of span

θ torsional rotation (twist), deg (see figs. 7 through 9)

$\Delta\theta/\Delta\alpha$ increment in torsional rotation per change in angle of attack

$\Delta\theta/\Delta\delta$ increment in torsional rotation per change in control-surface deflection

Θ torsional slope along 40 percent chord, rad (see fig. 5)

ϕ bending slope along 40 percent chord, rad

Subscripts:

ls lower surface

us upper surface

MODELS

Three models of the high-aspect-ratio, semispan wing are used in this study. They are the wind-tunnel model and two analytical models, namely, the finite-element structural model and the aerodynamic model.

Wind-Tunnel Model

The wind-tunnel model is shown mounted in the test section of the Langley Transonic Dynamics Tunnel in figure 1. A sketch showing some of the geometric details of the model is presented in figure 2. The model has an aspect ratio of 10.76, a leading-edge sweepback angle of 28.8°, and NASA supercritical-airfoil sections. Only 1 of the 10 control surfaces (number 9) was considered in this study. The wing model was designed and fabricated to be "rigid" by adding stiff boron-filament inserts to the aluminum wing-box construction as shown in figure 3. The model was attached to a five-component force balance which in turn was attached to a remotely controlled turntable mounted in the wind-tunnel wall. A complete description of the model is given in references 1 and 2.

Finite-Element Structural Model

An elastic-axis, finite-element structural model was constructed to represent the wind-tunnel semispan wing model. The finite-element model was developed using a system of computer programs called SPAR (now called EAL, Engineering Analysis Language). SPAR was designed primarily to perform stress, buckling, and vibrational analyses of linear finite-element systems (ref. 3). Figure 4 shows a sketch of the finite-element model used in this study. The model of the wing planform consists of 62 beam elements, 2 quadrilateral plates, and 1 zero-length beam spring element. These elements are positioned by nodal points which are listed in table 1. Twenty of the beam elements are along the elastic axis, the 40-percent-chord line. The stiffnesses of the 40-percent-chord beam elements were determined from laboratory measurements on the wind-tunnel model. The remaining beam elements were assigned a rigid stiffness (EI = 5.74 MPa; GJ = 2.87 MPa) and were oriented perpendicular to the elastic axis so that deflections at points off the elastic axis could be determined. The location of the nodal points for the beam elements along the elastic axis were selected to correspond to pressure-measurement stations and the locations midway between the pressure-measurement stations. The two quadrilateral plates model the control surface and were also assigned a rigid stiffness. The zero-length beam spring element represented the root-attachment flexibility, torsion and bending, of the model mounting system. The stiffnesses used for this element were also determined from laboratory measurements.

Measured and calculated structural data are presented in figure 5. These results were obtained by applying concentrated loads near the tip. A vertical load of 444.8 N (100 lbf), gave the measured and calculated bending-slope results shown in figure 5(a). A torsional load of 11.298 N-m (100 lbf-in.) gave the measured and

calculated torsional-slope results shown in figure 5(b). These results, determined along the elastic axis, indicate that the structural modeling of the wind-tunnel model was very accurate.

Aerodynamic Model

The aerodynamic model was generated by using linear subsonic lifting-surface theory as implemented through the RHOIV digital computer program (refs. 4 and 5). RHOIV was developed to calculate unsteady aerodynamic loadings caused by motions of lifting surfaces with leading-edge and trailing-edge control surfaces. RHOIV was selected to model the aerodynamics in this study because of its ability to incorporate control surfaces in its calculations and because of the ease with which it can be used.

For this study, steady-state aerodynamic loadings were determined from RHOIV when the reduced frequency was set to zero. A sketch of the RHOIV aerodynamic model is shown in figure 6. This figure shows the points used to define the planform shape. The locations of the collocation points used to calculate the pressures were determined through a default option available in RHOIV. This program treats the control surface and the wing separately and accounts for aerodynamic flow singularities of the control-surface hinge line. The aerodynamic model is a flat plate with the planform shape of the wind-tunnel model including one outboard trailing-edge control surface. When displacement points were used to represent a deformed wing shape, the location points were the same as the nodal points in the finite-element structural model.

ANALYSES

The finite-element structural model was combined with the RHOIV aerodynamic model to study the elastic deformation effects on the aerodynamic loading of the wing model at $M = 0.60$ and $M = 0.78$. The flow about the model at $M = 0.60$ was a subsonic test condition at which linear aerodynamic theory would be expected to be accurate. This aided in the comparison of experimental and analytical results. Mach 0.78, a transonic test condition, is the design Mach number for the wing. Analysis at both Mach numbers determined the deformations of the wing model due to a change in angle of attack and the aerodynamic characteristics due to these deformations. This analysis was also done at $M = 0.60$ for an increment of control-surface deflections. The aerodynamic load conditions were of two forms. One analysis used selected experimental pressure results from reference 2, and the other analysis used aerodynamic loads calculated by using the RHOIV aerodynamic model.

Analysis With Experimental Loads

The model deformations calculated from the experimentally determined wing-surface loadings were obtained by the following procedure. For the conditions of $M = 0.60$ and $q = 3.033$ kPa, the pressure distributions from reference 2 (points 159 and 214) were used. One set of data was for $\alpha = 2.85°$, and the other was for $\alpha = 0.0°$. The data were numerically integrated chordwise to obtain concentrated forces and moments at appropriate points along the 40-percent-chord line (elastic axis) of the wind-tunnel model. The concentrated loads were representative of a 1° change in angle of attack. The concentrated forces and moments were then applied to the corresponding nodal points of the structural model, and the resulting vertical

displacements and rotations along the elastic axis were calculated. This procedure was also for $M = 0.78$ ($q = 3.84$ kPa, $\alpha = 2.05°$ (point 63), and $\alpha = 0.0°$ (point 55)) and for $M = 0.60$ ($q = 3.052$ kPa, $\alpha = 2.85°$, $\delta = -6°$ (point 184), and $\delta = -2°$ (point 178)). (See ref. 2.)

Analysis With Theoretical Loads

The model deformations calculated from theoretically determined wing-surface loadings were obtained by using an iterative procedure. The RHOIV aerodynamic program was used to determine wing-surface pressure distributions for the same Mach numbers as the experimental loads analysis. However, at $M = 0.60$ and $M = 0.78$, the wing angle of attack was initially defined at 1°. Also, at $M = 0.60$ the wing angle of attack was initially defined at 0°, and the control surface was set at 1° deflection. The calculated pressure distributions were then converted to concentrated forces and moments along the elastic axis and applied to the finite-element model. The resulting deformation formed a new wing shape. The new wing shape was then used with the aerodynamic model to determine a new aerodynamic loading, which was applied to the finite-element model. The process was repeated until there was essentially no difference in the pressure distributions for successive iterations. In general, the process converged rapidly, requiring only two iterations.

DISCUSSION OF RESULTS

This investigation was conducted to determine the deflection characteristics of the wing model and to determine if these deflections had any effect on the aerodynamic characteristics. The analysis was conducted by using a finite-element structural model and an aerodynamic model, which were discussed previously. The results of the analysis are presented in the following sections.

Structural Results

A method of determining the rigidity of the wing model is to examine the deformations caused by aerodynamic loadings on the wing. As discussed in the section entitled "Analyses," two types of loads, experimental and theoretical, were applied to an accurate structural finite-element model of the wind-tunnel wing model. The deformations resulting from these loadings are shown in figures 7 through 9. Figure 7 shows the bending and torsional deflections for $M = 0.60$ at an incremental angle of attack. Similar results are shown in figure 8 for $M = 0.78$. In figure 9, the bending and torsional deflections are shown for $M = 0.60$ at an incremental control-surface deflection. The deformations shown in figures 7, 8, and 9(a) are, in general, similar in shape and value, although the theoretical and experimental load results are not in exact agreement. However, figure 9(b) shows a large discrepancy between the two load cases, the cause of which has not yet been determined. In all the figures, the differences between the theoretically and experimentally determined deformations are numerically small, but more importantly the overall deformations are considered very small. For example, at $M = 0.78$ for an incremental angle of attack the change in bending deflection is determined to be no more than 1.8 mm per angle of attack, and the change in rotation is not more than 0.025° per angle of attack at the tip where the greatest deflections occur. (See figs. 8(a) and 8(b).) The shape of the deflections along the wing span are similar to previous studies of wing deformations. (See ref. 6.) An attempt was made to measure actual deformations as they

occurred during the wind-tunnel tests by using a cathetometer. Unfortunately, the resolution of the cathetometer was not high enough to give accurate results.

Aerodynamic Results

Another method used to determine the rigidity of the wing model is to examine the effects the deformations had on some of the aerodynamic characteristics of the wing model. The results of this study are shown in figures 10 through 15.

As discussed in the section entitled "Analyses," an aerodynamic model was used with the RHOIV program to determine theoretically the pressure distribution over the wing model. Figures 10 through 12 show the pressure distributions at one of the semispan locations ($\eta = 0.71$) for the different Mach numbers with the incremental angle of attack and control-surface deflections for the experimental and theoretical loads. At $M = 0.60$ for an incremental angle of attack (fig. 10), three sets of data are shown, the experimental data, the data from the aerodynamic model without deformations, and the data from the aerodynamic model with the final deformations of the iterative procedure. As can be seen, there is fairly close agreement between the experimental data and the two sets of theoretical data. The close agreement between the two sets of theoretical data shows that the deformations created by the aerodynamic loads do not significantly affect the pressures at this semispan location of the wing. Similar results at an incremental angle of attack for $M = 0.78$ and at an incremental control-surface deflection for $M = 0.60$ are shown in figures 11 and 12, respectively. In all three figures there is some disagreement between the experimentally and theoretically determined data. Some of the discrepancy could be due to slight scatter, but another source of slight error comes from the RHOIV aerodynamic program. As the program was initially used, the dynamic pressure distributions at transonic Mach numbers and over control-surface hinge lines did not give as accurate results as are now available (ref. 5); however, the results achieved were considered adequate for this study.

Figures 13 through 15 show the change in section lift coefficient and section pitching-moment coefficient over the wing span at $M = 0.60$ for an incremental angle of attack, $M = 0.78$ for an incremental angle of attack, and $M = 0.60$ for an incremental control-surface deflection, respectively. The experimental and theoretical pressure data were integrated over the wing chords to give these results, which were used with the finite-element structural model to determine the deformed shape of the wing model. At $M = 0.60$ for an incremental angle of attack (fig. 13), there is fairly close agreement for the section lift coefficient over the wing span. There is much more scatter in figure 13(b) for the section pitching-moment coefficient over the wing span. Some of this scatter, as in figures 14 and 15, may have resulted from some nonlinearity between angles of attack and control-surface deflections in determining the lifts and moments for incremental values. Figure 14 shows the section lift and pitching-moment coefficients at $M = 0.78$ for an incremental angle of attack. In figures 14(a) and 14(b), there is still some disagreement between the experimental and theoretical cases, although there is better agreement for the moment at $M = 0.78$ than at $M = 0.60$. Also, the two sets of theoretical data compare well for the section lift and pitching-moment coefficients. Figure 15 shows the section lift and pitching-moment coefficients at $M = 0.60$ for an incremental control-surface deflection. These results are similar to those already presented. However, there are only two sets of data in figure 15(b). The theoretical data with the deformation effects for an incremental section pitching-moment coefficient were not available.

SUMMARY OF RESULTS

The concerns that the wind-tunnel model would experience deformations and that these deformations would affect the aerodynamic characteristics of the wing have been addressed and examined through two methods of analysis. The results of this study indicate the following:

1. The deformations of the wing model are very small. That is, the maximum deflections are at $M = 0.78$, where the increment in bending deflection per change in angle of attack is 1.61 mm/deg and the increment in torsional rotation per change in angle of attack is ~~2.085~~ 0.02085.

2. There is good agreement between the theoretical and experimental pressure data.

3. The iterative procedure used to calculate the theoretical aerodynamic characteristics shows that there is little difference between the results for the deflected and nondeflected wing models.

4. The good agreement between the theoretical and experimental aerodynamic data and the close agreement between the theoretical aerodynamic results for the deflected and nondeflected model shapes shows that the deformations do not significantly affect the aerodynamic characteristics of the wing model.

Langley Research Center
National Aeronautics and Space Administration
Hampton, VA 23665
April 14, 1982

REFERENCES

1. Sandford, Maynard C.; Ricketts, Rodney H.; and Cazier, F. W., Jr.: Transonic Steady- and Unsteady-Pressure Measurements on a High-Aspect-Ratio Supercritical-Wing Model With Oscillating Control Surfaces. NASA TM-81888, 1980.

2. Sandford, Maynard C.; Ricketts, Rodney H.; and Watson, Judith J.: Subsonic and Transonic Pressure Measurements on a High-Aspect-Ratio Supercritical-Wing Model With Oscillating Control Surfaces. NASA TM-83201, 1981.

3. Whetstone, W. D.: SPAR Structural Analysis System Reference Manual - System Level 13A. Volume I: Program Execution. NASA CR-158970-1, 1978.

4. Petrarca, J. R.; Harrison, B. A.; Redman, M. C.; and Rowe, W. S.: Reduction of Computer Usage Costs in Predicting Unsteady Aerodynamic Loadings Caused by Control Surface Motions. NASA CR-145354, 1979.

5. Rowe, W. S.; and Petrarca, J. R.: Reduction of Computer Usage Costs in Predicting Unsteady Aerodynamic Loadings Caused by Control Surface Motions - Addendum to Computer Program Description. NASA CR-145354-1, 1980.

6. Brooks, Joseph D.; and Beamish, Jerry K.: Measurement of Model Aeroelastic Deformations in the Wind Tunnel at Transonic Speeds Using Stereophotogrammetry. NASA TP-1010, 1977.

TABLE 1.- NODAL POINTS FOR FINITE-ELEMENT MODEL

Nodal points	x, m	y, m	z, m
Leading edge			
1	0.00	0.00	0.00
2	.171	.310	
3	.273	.502	
4	.305	.559	
5	.324	.597	
6	.343	.622	
7	.349	.641	
8	.400	.730	
9	.451	.813	
10	.514	.940	
11	.565	1.022	
12	.673	1.225	
13	.800	1.454	
14	.921	1.670	
15	.965	1.753	
16	1.003	1.829	
17	1.022	1.861	
18	1.035	1.886	
19	1.105	2.013	
20	1.175	2.140	
21	1.256	2.286	
Elastic axis (40 percent)			
22	0.320	0.00	0.00
23	.403	.219	
24	.484	.432	
25	.501	.477	
26	.518	.521	
27	.527	.547	
28	.537	.573	
29	.573	.666	
30	.608	.760	
31	.652	.876	
32	.695	.966	
33	.794	1.172	
34	.903	1.401	
35	1.013	1.629	
36	1.051	1.710	
37	1.090	1.791	
38	1.102	1.816	
39	1.118	1.842	
40	1.176	1.971	
41	1.238	2.099	
42	1.328	2.286	

TABLE 1.- Concluded

Nodal point	x, m	y, m	z, m
Trailing edge			
43	0.800	0.00	0.00
44	.813	.064	
45	.838	.298	
46	.844	.343	
47	.851	.394	
48	.851	.419	
49	.864	.451	
50	.876	.552	
51	.889	.654	
52	.895	.787	
53	.907	.876	
54	.984	1.079	
55	1.079	1.314	
56	1.112	1.571	
57	1.147	1.658	
58	1.181	1.739	
59	1.194	1.769	
60	1.204	1.795	
61	1.304	1.911	
62	1.359	2.045	
63	1.447	2.286	
Control surface			
64	1.087	1.346	-0.0011
65	1.172	1.569	-.0010
66	1.265	1.811	-.0008
67	1.018	1.346	.00
68	1.112	1.572	.00
69	1.213	1.816	.00
Root cantilever spring element			
70	0.320	0.00	0.00

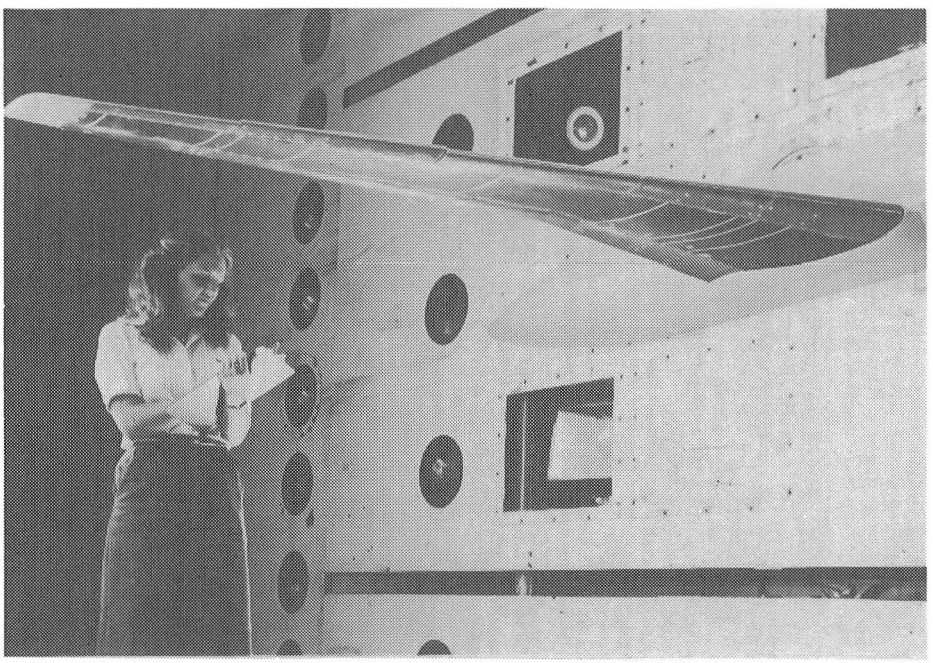

L-82-136

Figure 1.- Wing model mounted in wind tunnel.

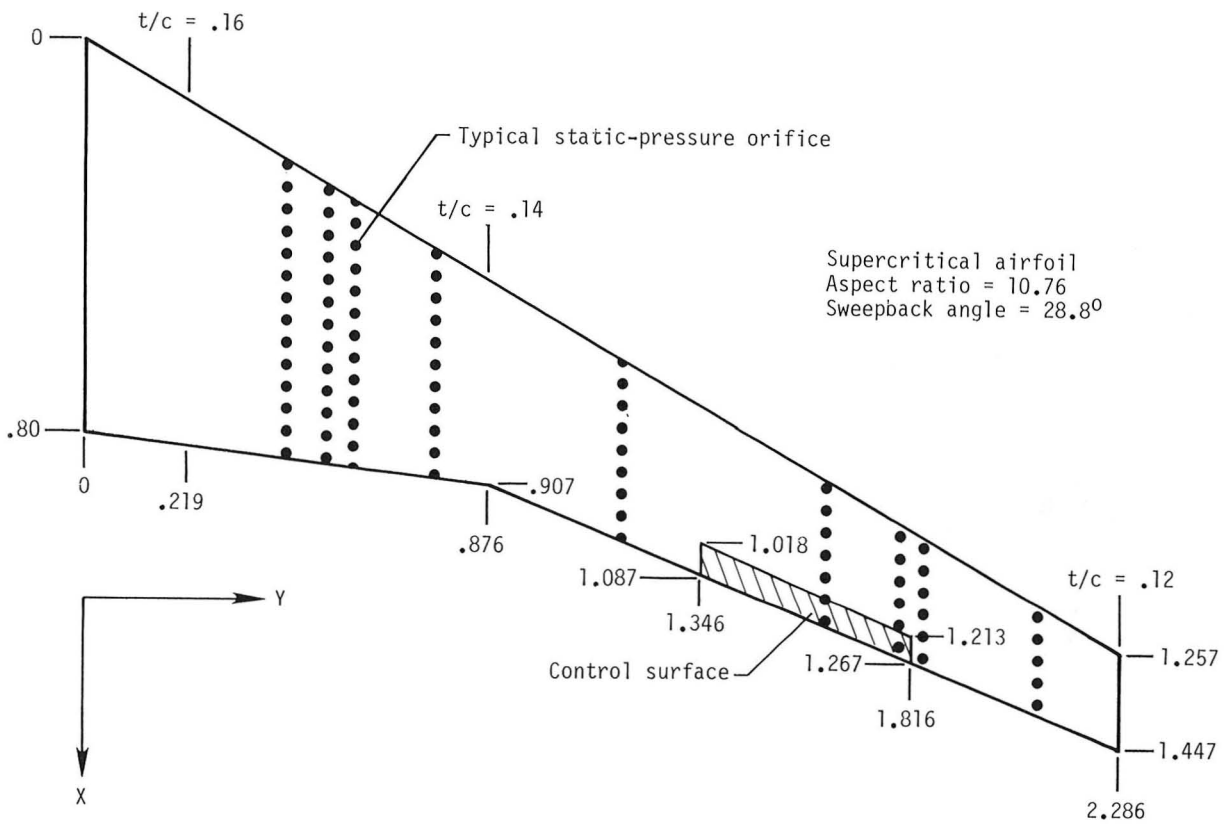

Figure 2.- Sketch of high-aspect-ratio wing model. Linear dimensions in meters.

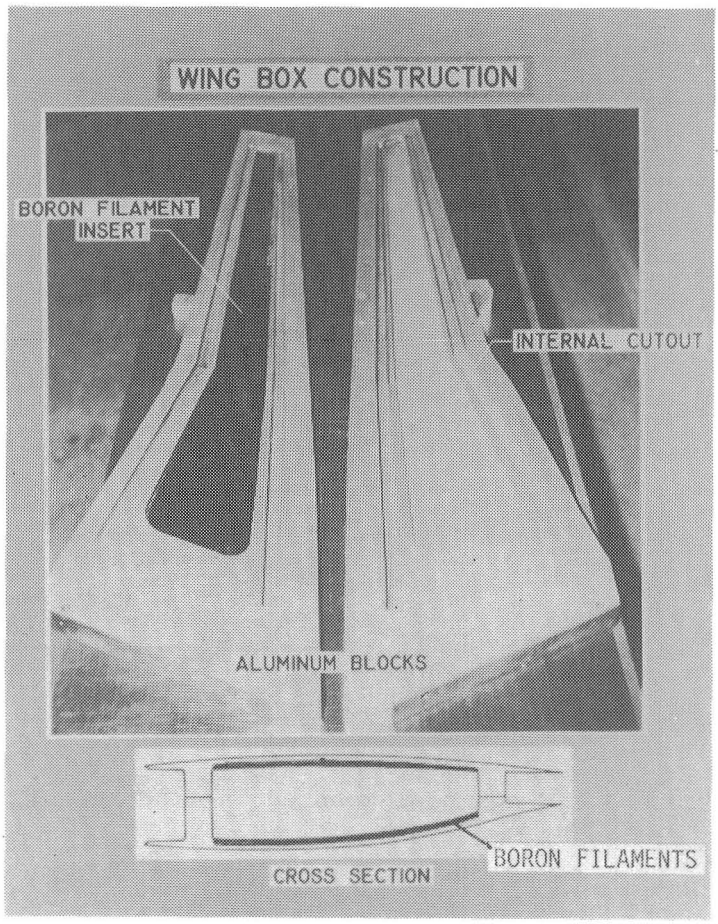

L-82-137

Figure 3.- Wing-box construction details.

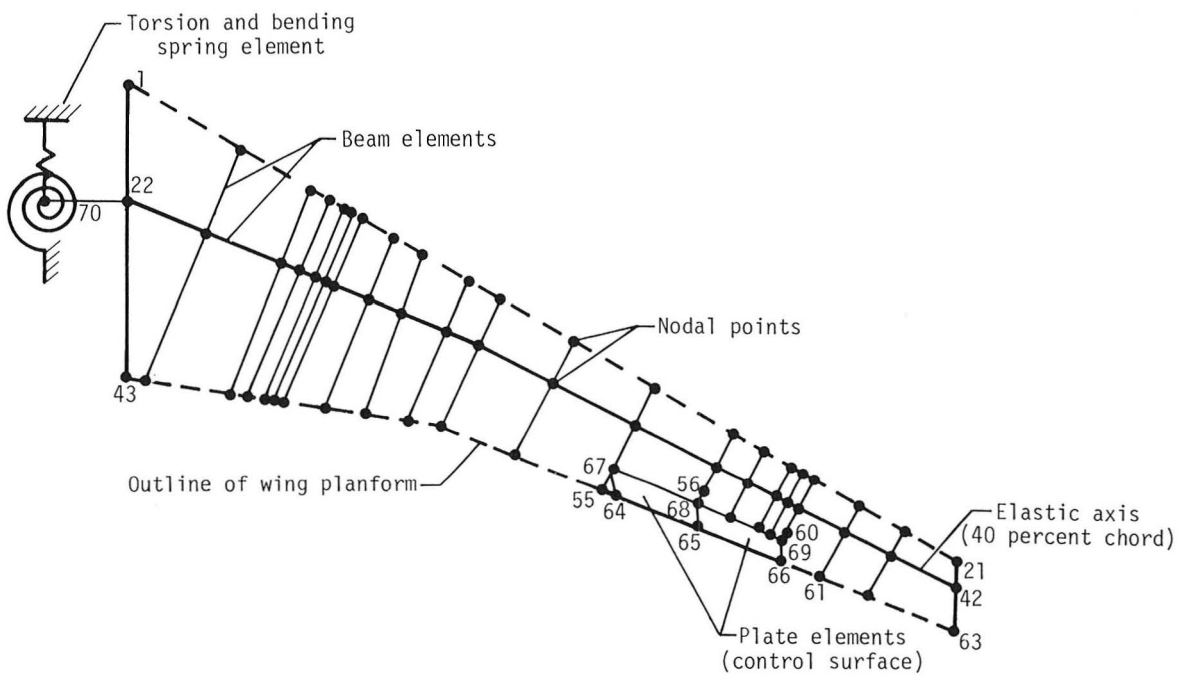

Figure 4.- Sketch of SPAR finite-element structural model. (See table 1.)

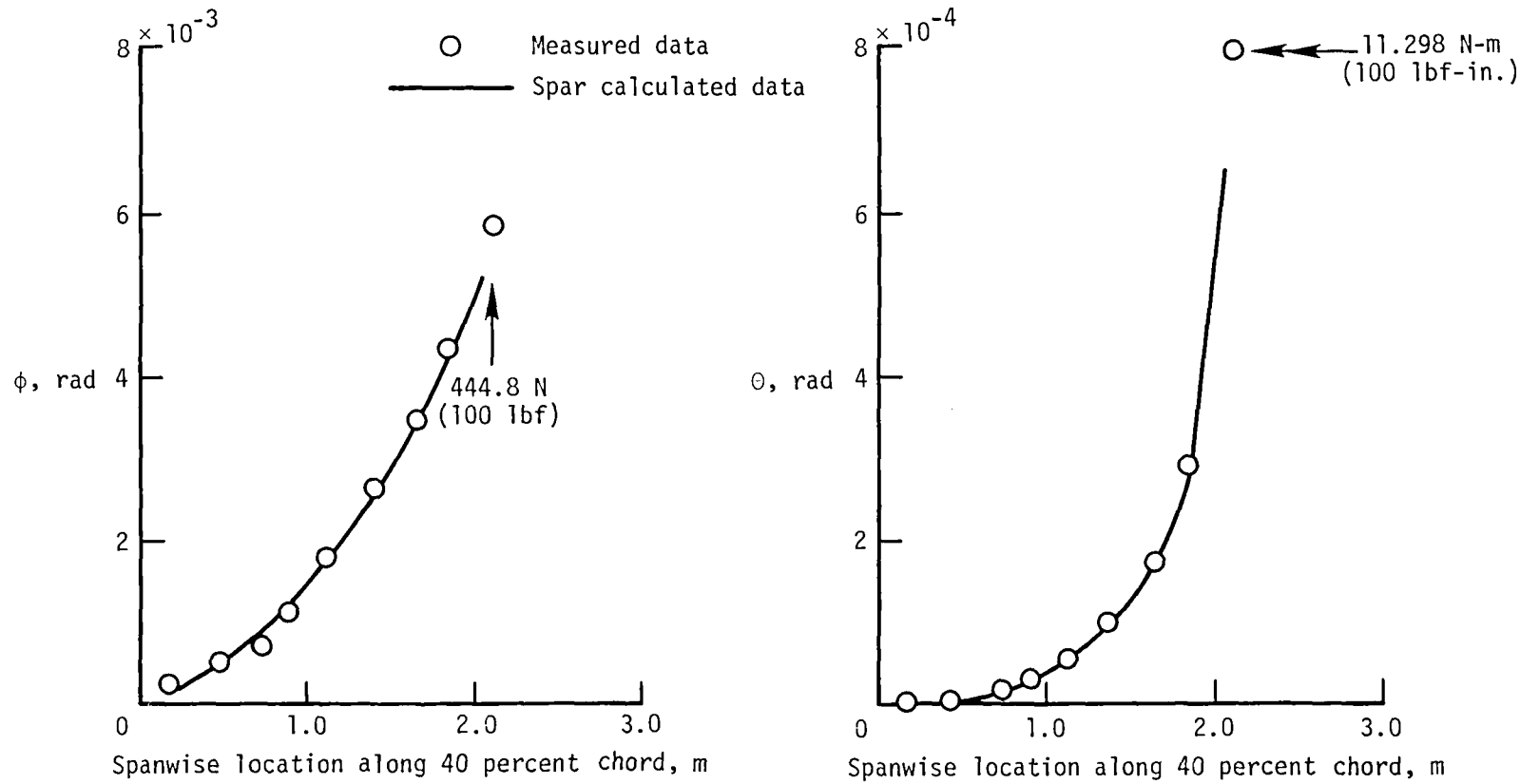

(a) Bending slope.

(b) Torsional rotation.

Figure 5.- Comparison of finite-element-determined deformations with measured deformations of wind-tunnel model.

Collocation point locations

Y_{1-6}	X_1	X_2	X_3	X_4	X_5	X_6
2.220	1.232	1.264	1.309	1.357	1.397	1.419
2.024	1.127	1.164	1.217	1.272	1.319	1.345
1.711	.959	1.004	1.069	1.137	1.194	1.226
1.299	.735	.792	.871	.956	1.026	1.066
.811	.471	.543	.644	.753	.842	.893
.276	.189	.298	.451	.614	.749	.826

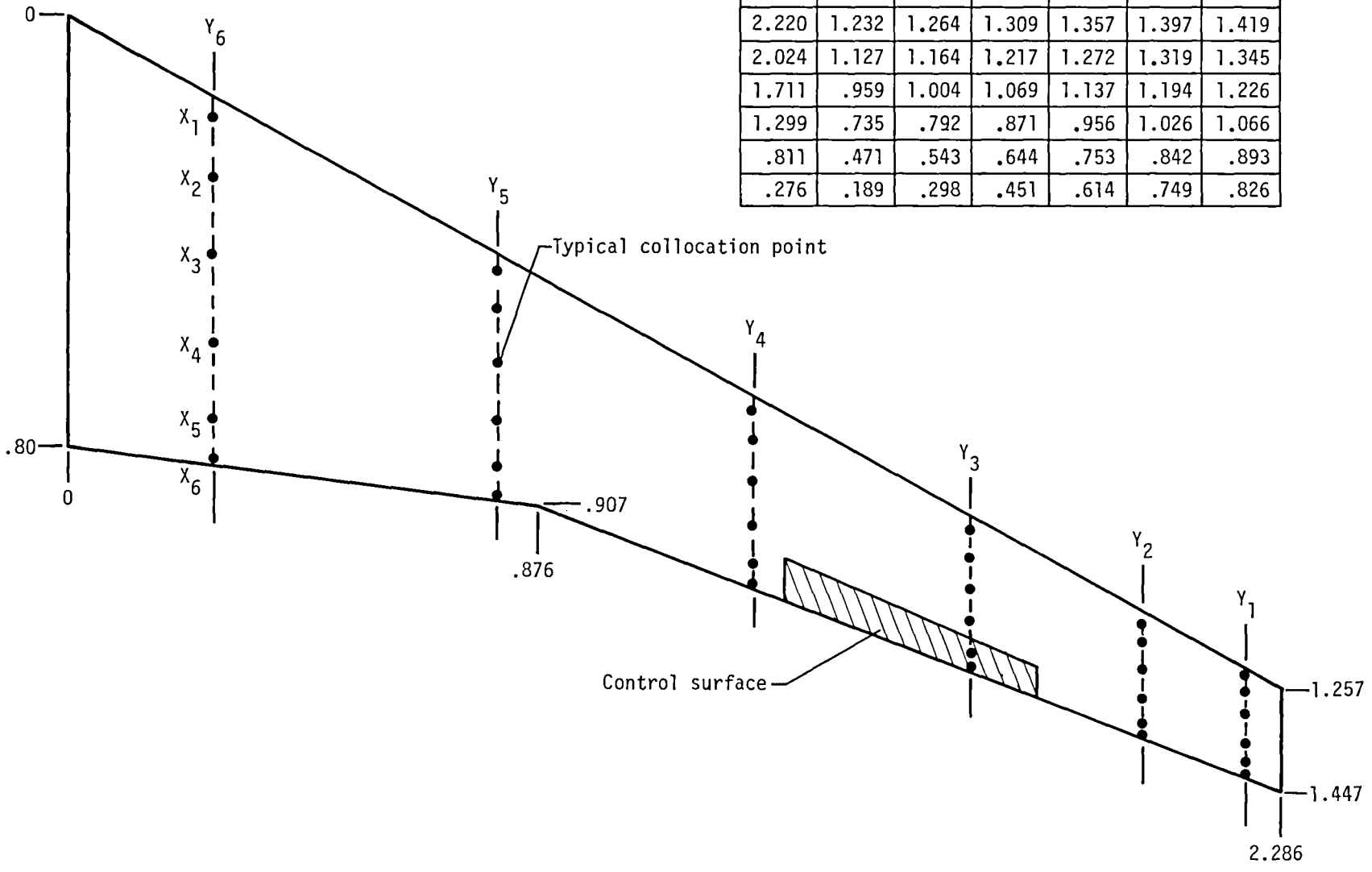

Figure 6.- Sketch of RHOIV aerodynamic model. Dimensions in meters.

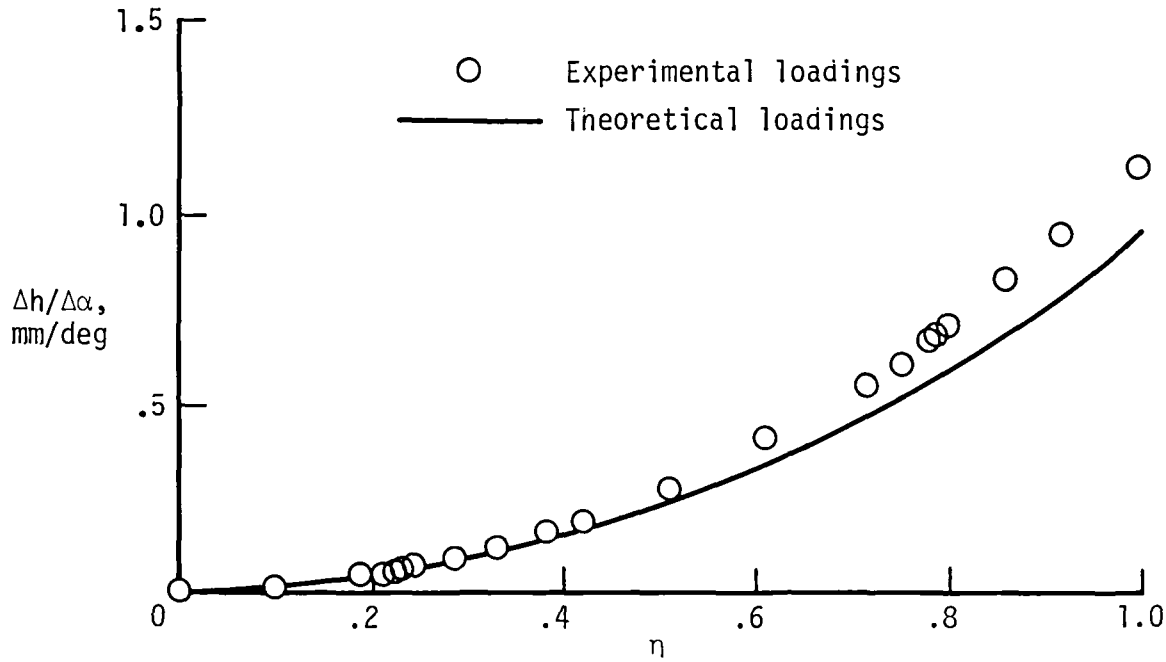

(a) Bending deflections.

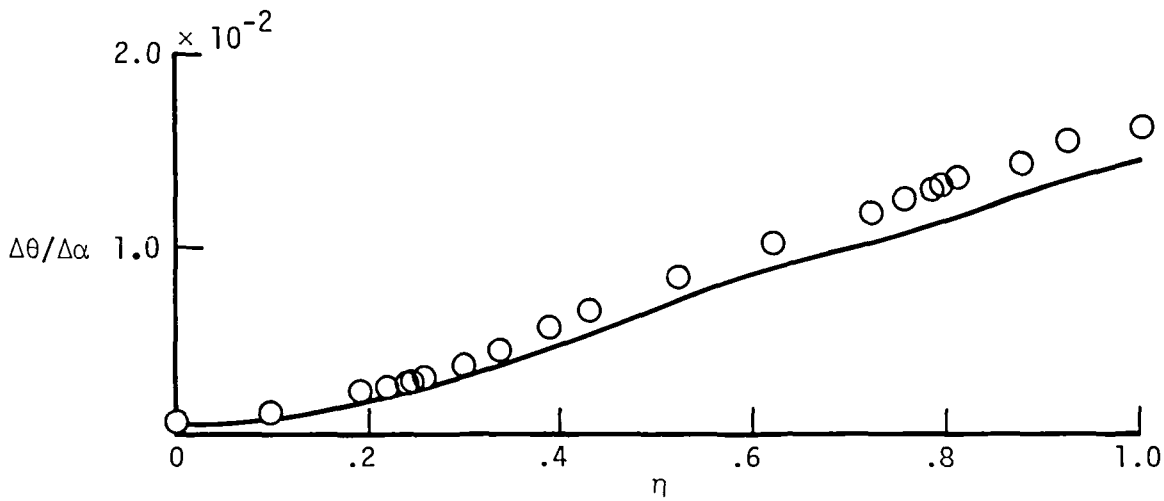

(b) Torsional deflections.

Figure 7.- Incremental spanwise deflections of wing along 40 percent chord at M = 0.60 for an incremental angle of attack.

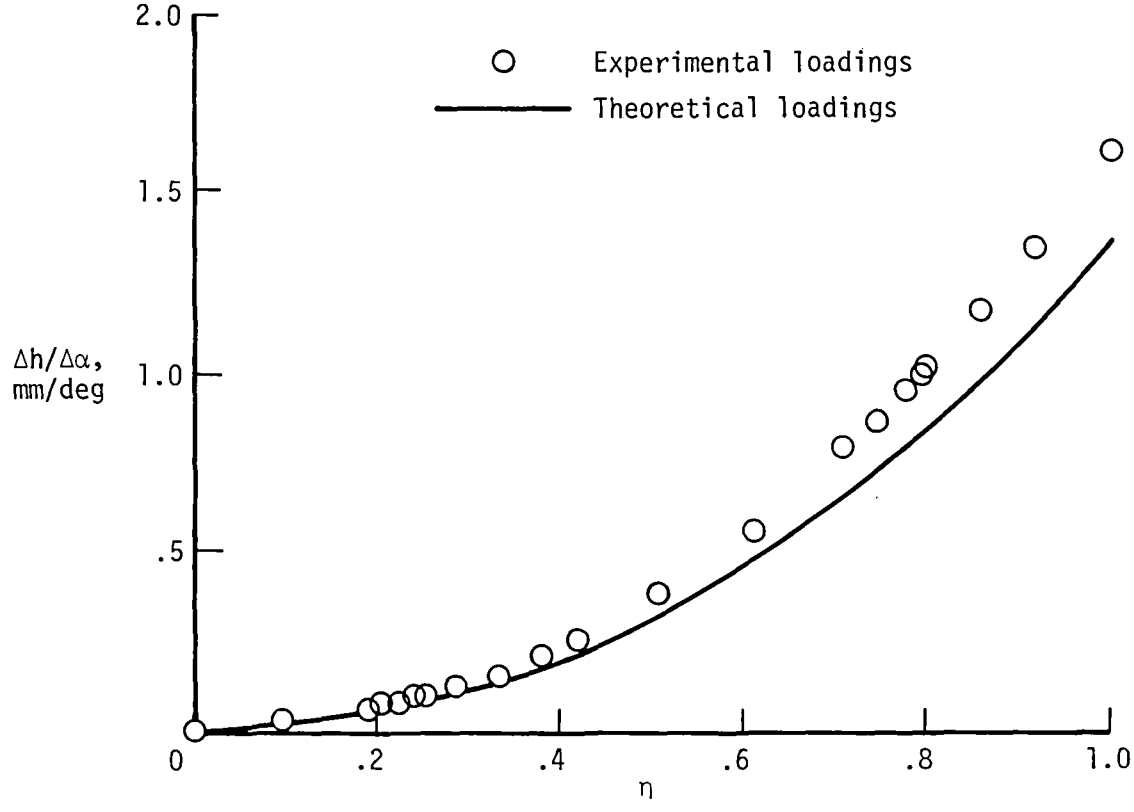

(a) Bending deflections.

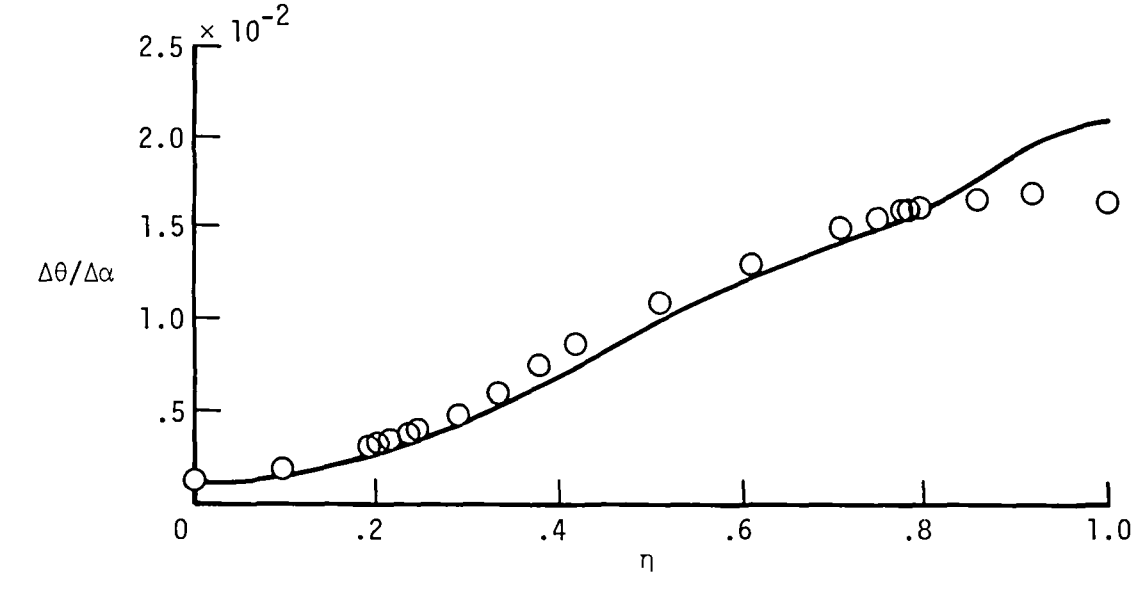

(b) Torsional deflections.

Figure 8.- Incremental spanwise deflections of wing along 40 percent chord at M = 0.78 for an incremental angle of attack.

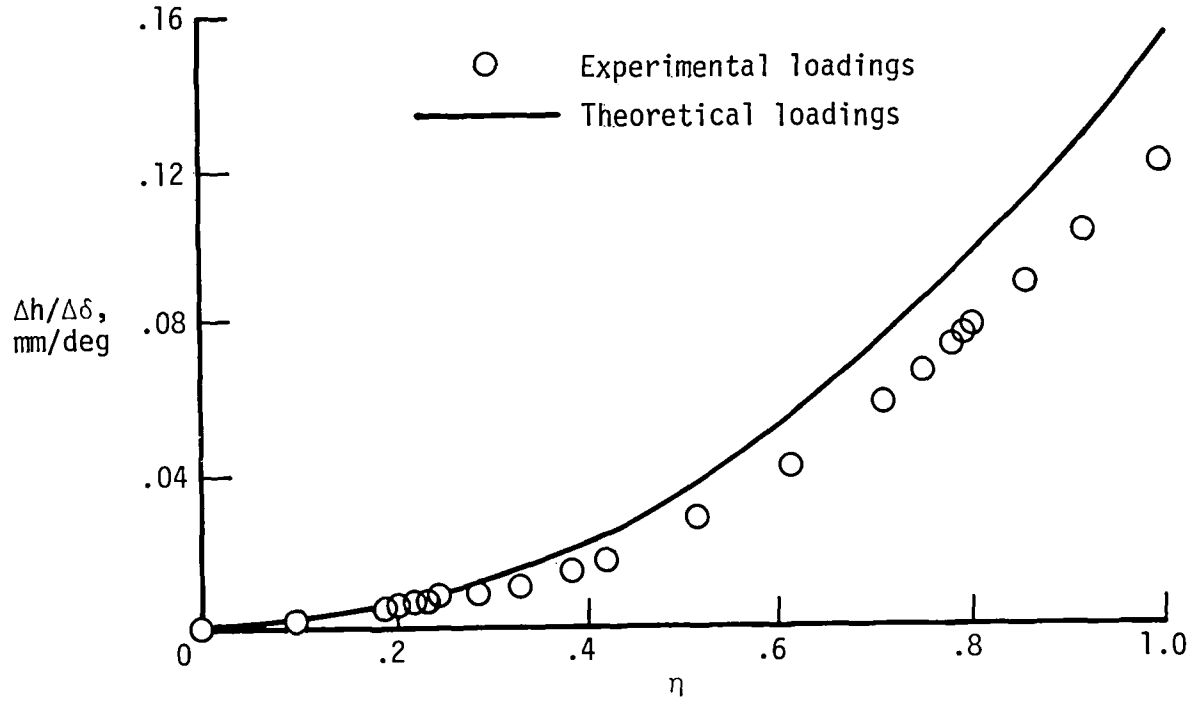

(a) Bending deflections.

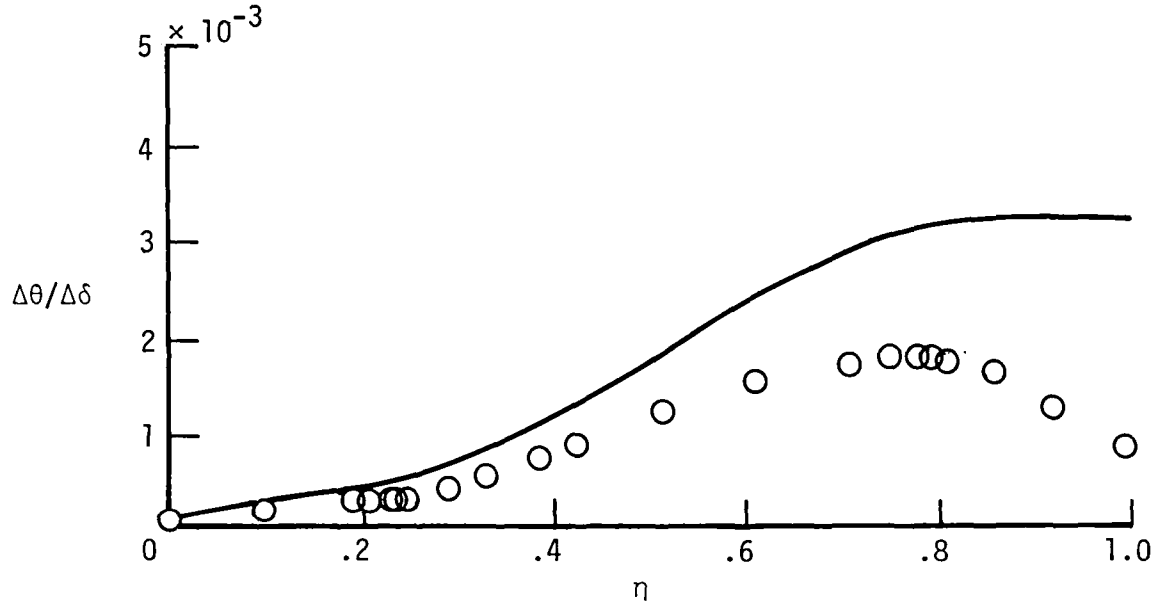

(b) Torsional deflections.

Figure 9.- Incremental spanwise deflections of wing along 40 percent chord at M = 0.60 for an incremental control-surface deflection.

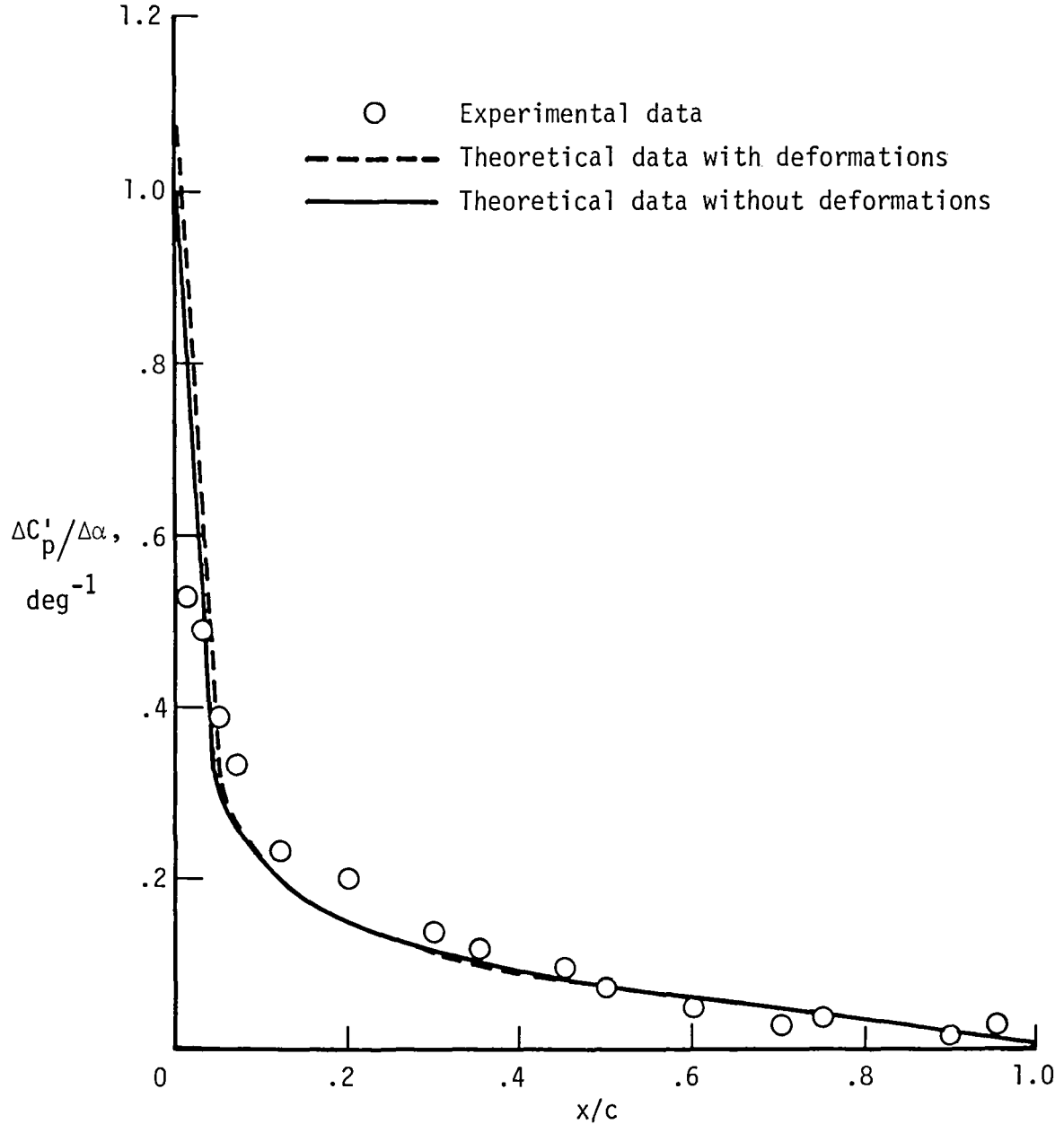

Figure 10.- Incremental lifting-surface pressure distribution at $\eta = 0.71$ and $M = 0.60$ for an incremental angle of attack.

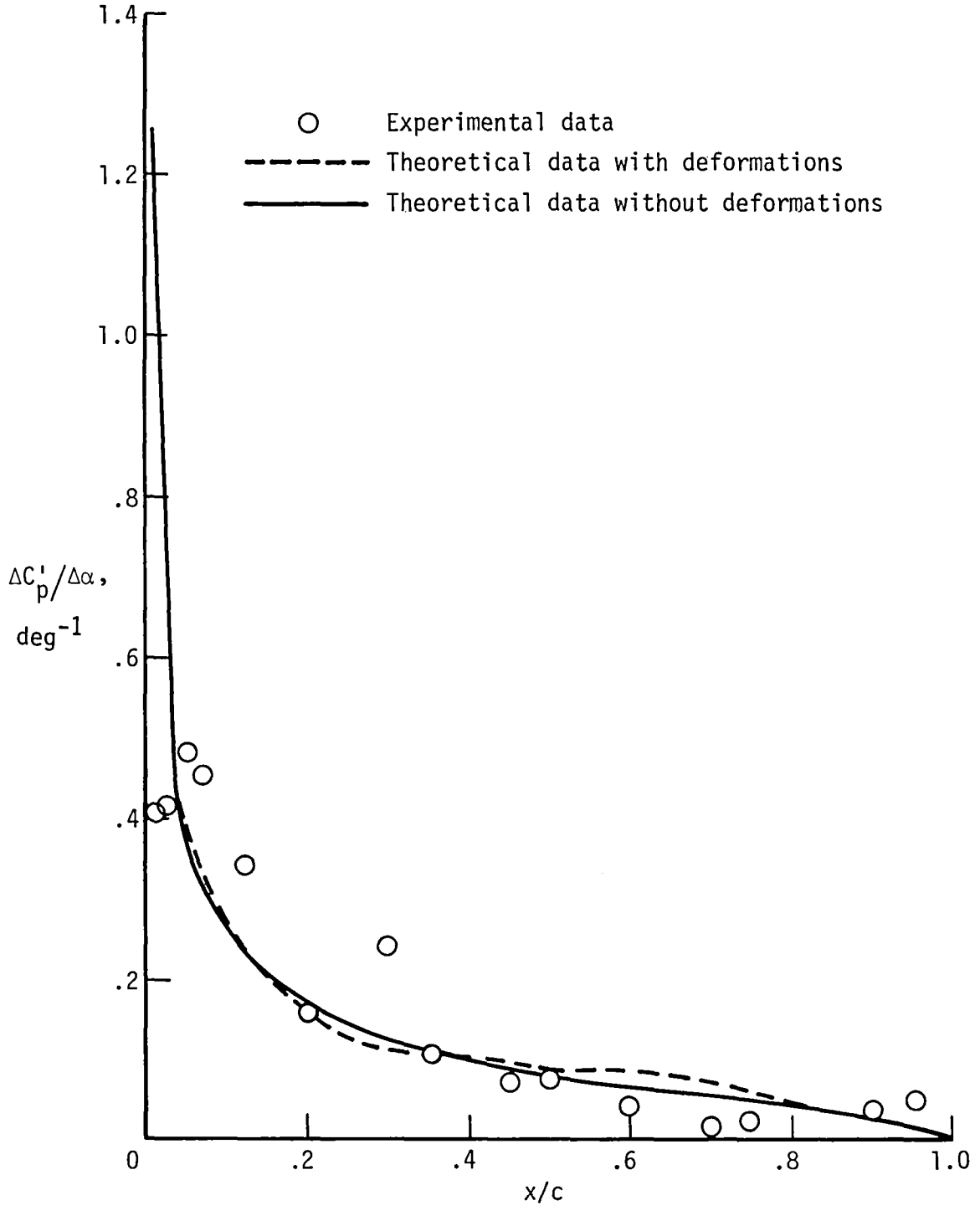

Figure 11.- Incremental lifting-surface pressure distribution at $\eta = 0.71$ and $M = 0.78$ for an incremental angle of attack.

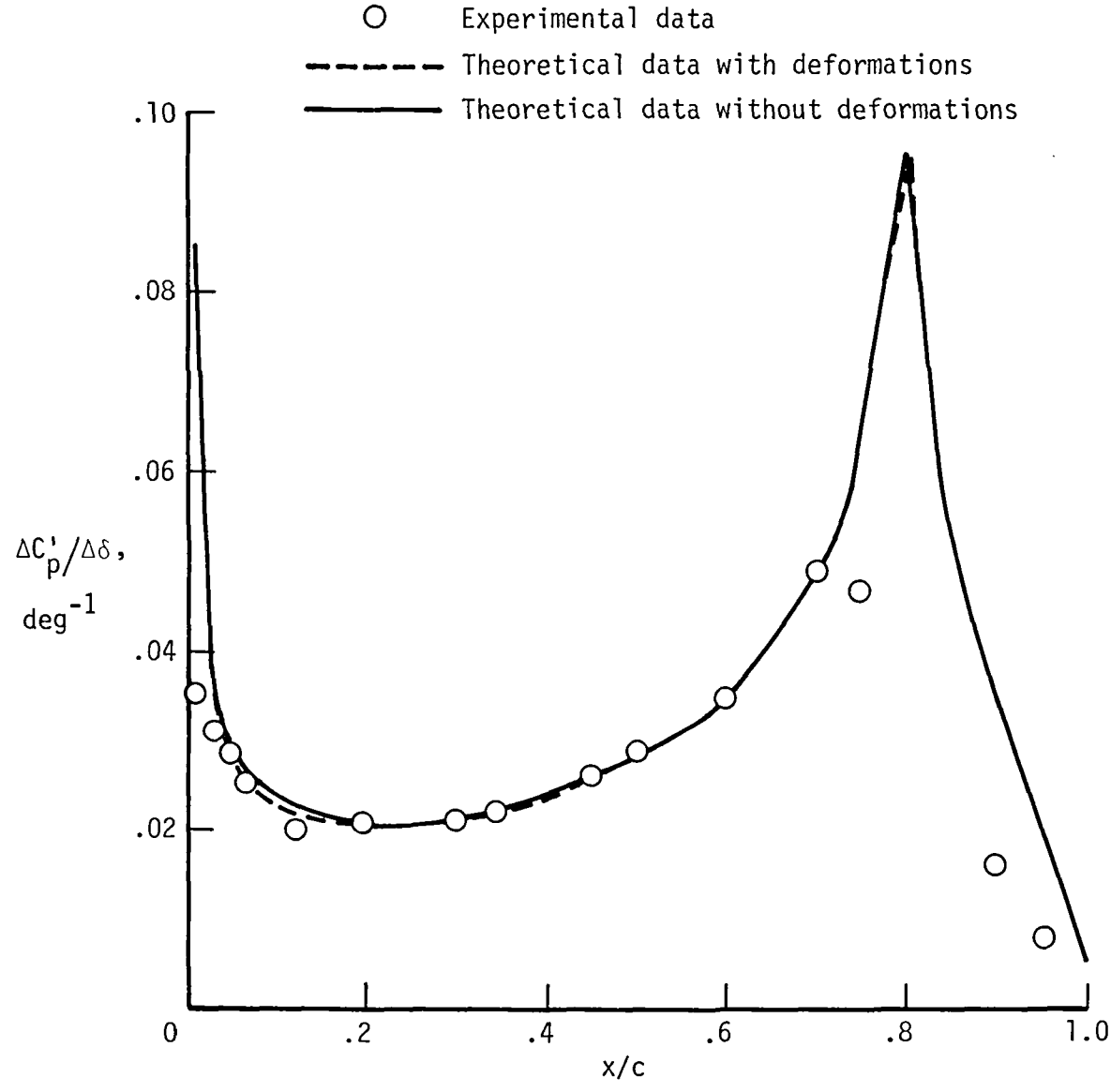

Figure 12.- Incremental lifting-surface pressure distribution at $\eta = 0.71$ and $M = 0.60$ for an incremental control-surface deflection.

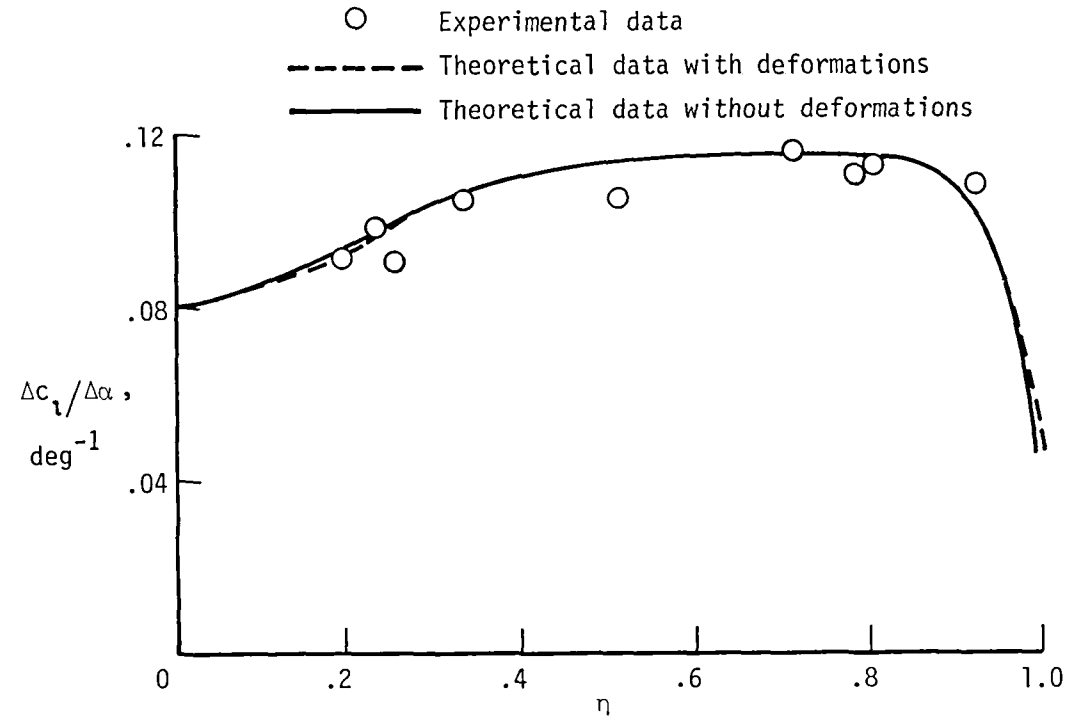

(a) Incremental section lift coefficient.

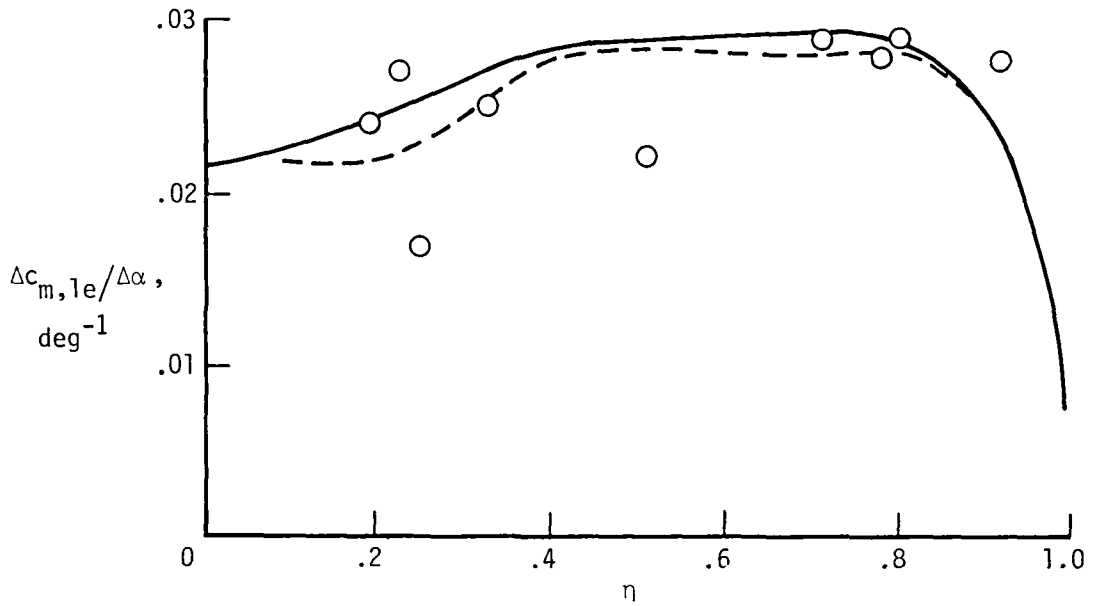

(b) Incremental section pitching-moment coefficient.

Figure 13.- Spanwise aerodynamic characteristics of wing model at M = 0.60 for an incremental angle of attack.

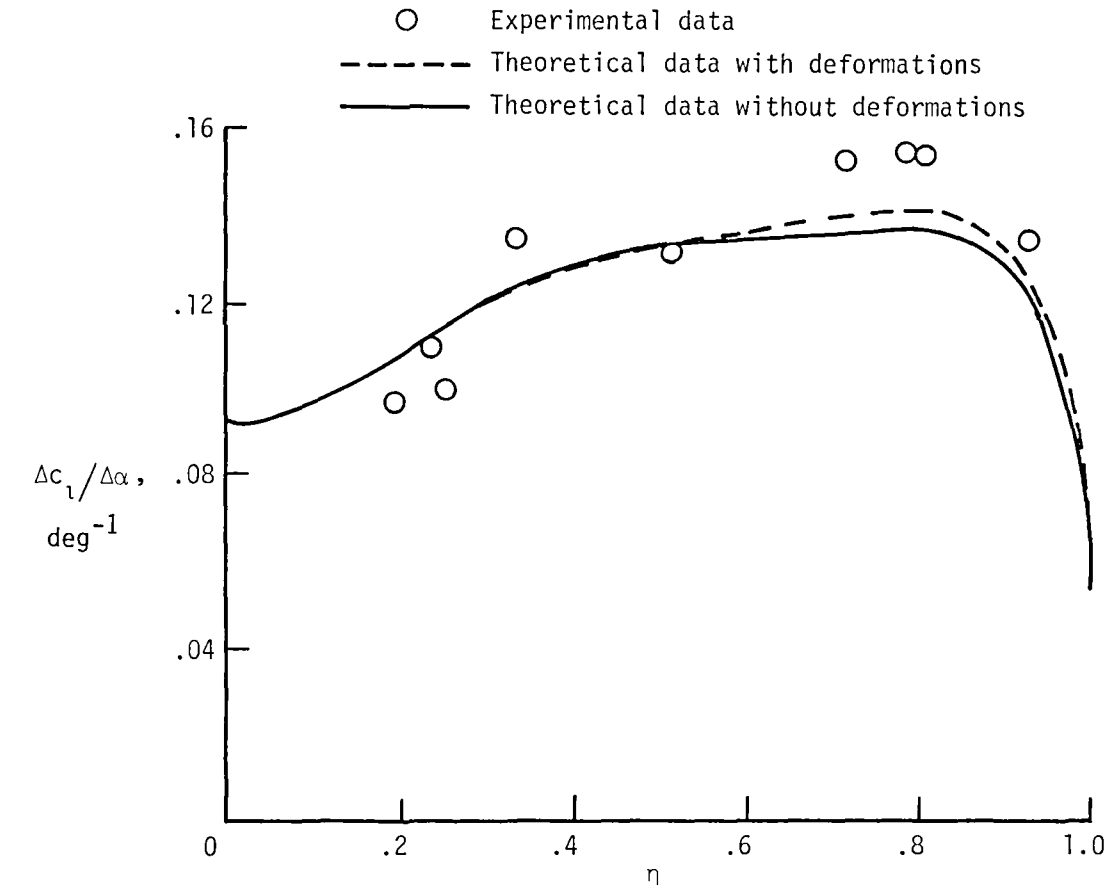

(a) Incremental section lift coefficient.

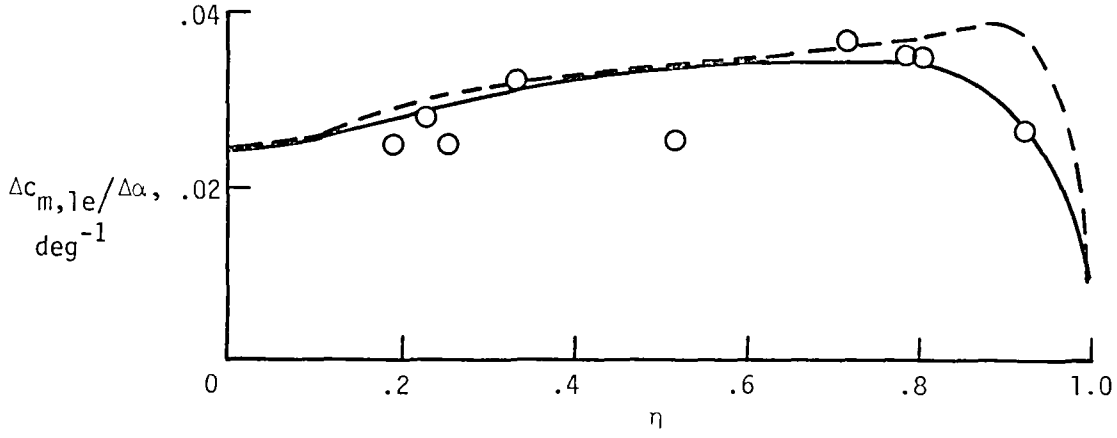

(b) Incremental section pitching-moment coefficient.

Figure 14.- Spanwise aerodynamic characteristics of wing model at M = 0.78 for an incremental angle of attack.

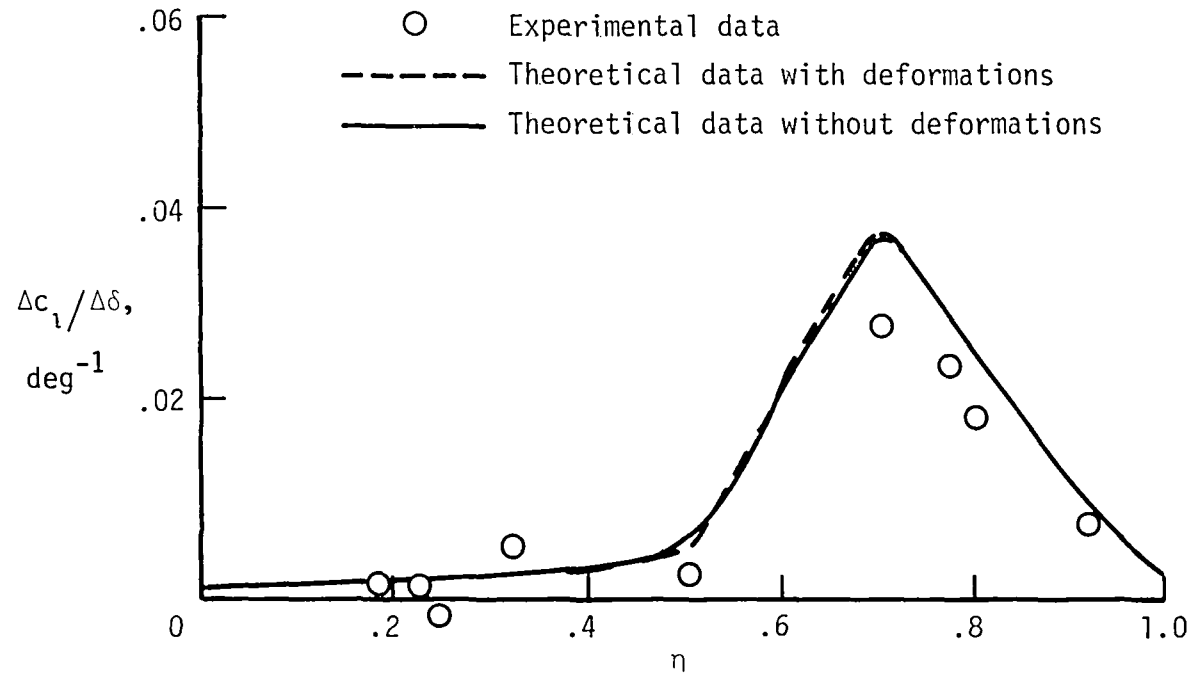

(a) Incremental section lift coefficient.

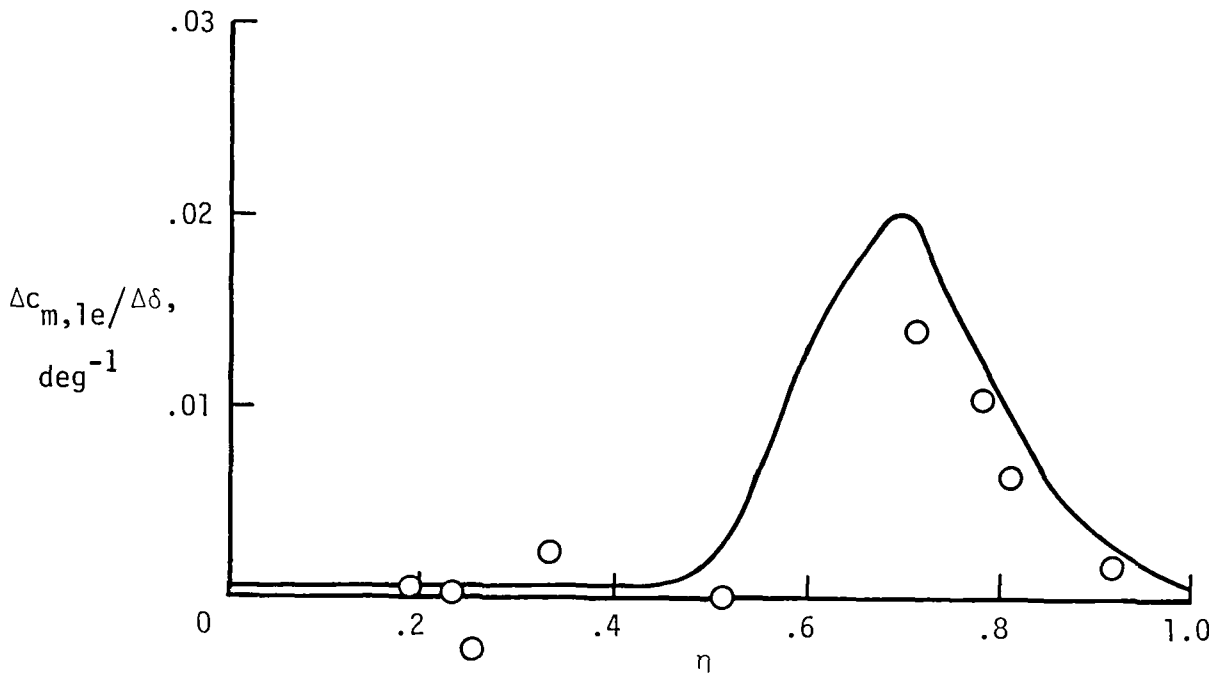

(b) Incremental section pitching-moment coefficient.

Figure 15.- Spanwise aerodynamic characteristics of wing model at M = 0.60 for an incremental control-surface deflection.

1. Report No.	2. Government Accession No.	3. Recipient's Catalog No.
NASA TM-83286		

4. Title and Subtitle	5. Report Date
ELASTIC DEFORMATION EFFECTS ON AERODYNAMIC CHARACTERISTICS FOR A HIGH-ASPECT-RATIO SUPERCRITICAL-WING MODEL	May 1982
	6. Performing Organization Code: 534-02-13-21
7. Author(s): Judith J. Watson	8. Performing Organization Report No.: L-15098
	10. Work Unit No.
9. Performing Organization Name and Address: NASA Langley Research Center, Hampton, VA 23665	11. Contract or Grant No.
	13. Type of Report and Period Covered: Technical Memorandum
12. Sponsoring Agency Name and Address: National Aeronautics and Space Administration, Washington, DC 20546	14. Sponsoring Agency Code

15. Supplementary Notes

16. Abstract

This paper presents the results of an investigation of the deformations of a high-aspect-ratio, force/pressure, supercritical-wing model during wind-tunnel tests and the effects these deformations have on the wing aerodynamics. A finite-element model of the wing was developed, and then, for conditions corresponding to wind-tunnel test points, experimental aerodynamic loads and theoretical aerodynamic loads were applied to the finite-element model. Comparisons were made between the results of these load conditions for changes in structural deflections and for changes in aerodynamic characteristics. The results showed that the deformations were quite small and that the pressure data were not significantly affected by model deformation.

17. Key Words (Suggested by Author(s))	18. Distribution Statement
Flexibility effects Elastic deformation Supercritical-wing model Wind-tunnel model	Unclassified - Unlimited Subject Category 02

19. Security Classif. (of this report)	20. Security Classif. (of this page)	21. No. of Pages	22. Price
Unclassified	Unclassified	24	A02

For sale by the National Technical Information Service, Springfield, Virginia 22161

NASA-Langley, 1982

National Aeronautics and
Space Administration

Washington, D.C.
20546

Official Business
Penalty for Private Use, $300

THIRD-CLASS BULK RATE

Postage and Fees Paid
National Aeronautics and
Space Administration
NASA-451

NASA

POSTMASTER: If Undeliverable (Section 158
Postal Manual) Do Not Return